This is the accepted manuscript made available via CHORUS. The article has been published as:

Current-induced dynamics and tunable spectra of a magnetic chiral bobber

Zizhao Gong, Jin Tang, Sergey S. Pershoguba, Zongkai Xie, Rui Sun, Yang Li, Xu Yang, Jianan Liu, Wei Zhang, Xiangqun Zhang, Wei He, Haifeng Du, Jiadong Zang, and Zhao-hua Cheng

Phys. Rev. B **104**, L100412 — Published 17 September 2021

DOI: 10.1103/PhysRevB.104.L100412

Current-Induced Dynamics and Tunable Spectra of a Magnetic Chiral Bobber

Zizhao Gong,[1, 2] Jin Tang,[3] Sergey S. Pershoguba, [4] Zongkai Xie,[1, 2] Rui Sun,[1, 2] Yang Li,[1, 2] Xu Yang,[1, 2] Jianan Liu,[1, 2] Wei Zhang,[1] Xiangqun Zhang,[1] Wei He,[1] Haifeng Du,[3, 5] Jiadong Zang,[4, 6,*] and Zhao-hua Cheng[1, 2, 7, †]

[1]*State Key Laboratory of Magnetism and Beijing National Laboratory for Condensed Matter Physics, Institute of Physics, Chinese Academy of Sciences, Beijing 100190, China*

[2]*School of Physical Sciences, University of Chinese Academy of Sciences, Beijing 100049, China*

[3]*The Anhui Province Key Laboratory of Condensed Matter Physics at Extreme Conditions, High Magnetic Field Laboratory, Chinese Academy of Sciences and University of Science and Technology of China, Hefei 230026, China*

[4]*Department of Physics and Astronomy, University of New Hampshire, Durham, New Hampshire 03824, USA*

[5]*Department of Physics, School of Physics and Materials Science, Anhui University, Hefei 230601, China*

[6]*Materials Science Program, University of New Hampshire, Durham, New Hampshire 03824, USA*

[7]*Songshan Lake Materials Laboratory, Dongguan, Guangdong 523808, China*

Abstract

Chiral bobber (ChB) is an exotic three-dimensional topological texture in chiral magnets. It is composed of a Bloch point (BP) singularity and a skyrmion tube; the incommensurate characteristic length scales of these two components would thus lead to novel dynamics of a ChB. Here, we report the current-induced motion and the accompanying Hall effect of a ChB. Surprisingly, we find that the Hall angle of a ChB can be tuned in a wide range from -90° to positive angles. A further study of spin wave excitations identified high-frequency resonant modes, which are related to the velocity of ChB and lattice constants. The excited frequency can be two orders of magnitude higher than that of skyrmions. The broad ranges of Hall angles and frequency spectra could boost the development of spintronic devices using topological textures.

Corresponding authors:

[†]zhcheng@iphy.ac.cn

[*]Jiadong.Zang@unh.edu

Introduction

Chiral bobber (ChB)[1-3] is a stable three-dimensional composite quasiparticle residing in proximity to the surface of chiral magnets. As shown in Fig. 1, it may be visualized as a skyrmion tube[4,5] of variable diameter, which decreases progressively from the chiral magnet surface to the interior and finally shrinks into a magnetic singularity, the so-called Bloch point (BP)[6-9]. We characterize a ChB by the diameter of the skyrmion tube at the surface L_d and the bobber length L_p. Owing to its particle-like nature, ChB has been suggested as an information carrier in spintronic devices. In addition, it was demonstrated [10] that terahertz radiation can arise from BP dynamics in chiral magnets. Theoretical prediction [1] and experimental observations[2,3] call for a thorough investigation of the dynamical properties of ChB. Recently, methods for creating single ChB[11] and ChB lattice[12] were identified. Confined BPs in the form of a pair of opposing ChBs were predicted[8] further suggesting that the unique magnetic structure of ChBs may contain a wealth of physical phenomena.

Over the years, fundamental physical properties and potential applications, e.g. the current-driven motion and excitation spectrum, for novel magnetic structures[13-30] have been studied extensively. On the other hand, although the concept of ChB has been known for several years, many physical properties are still largely unexplored. In this context, it is important to address the current-induced dynamics of ChB, which is the main focus of this work.

Although the ChB has high energy associated with the singularity, it is protected by a significant barrier due to the nontrivial topology of both the skyrmion and BP in terms of the same homotopy mapping, $\pi_2(S^2)$. The corresponding topological charge is

$$q = \frac{1}{8\pi}\int dA_i \epsilon_{ijk} \boldsymbol{m} \cdot \partial_j \boldsymbol{m} \times \partial_k \boldsymbol{m} \qquad (1)$$

where $\boldsymbol{m}(\boldsymbol{r}) = (sin\theta cos\phi, sin\theta sin\phi, cos\theta)$ is the unit vector in the direction of local magnetization. For a skyrmion, the integral is performed over the two-dimensional plane, whereas for a BP, the integral is carried over a surrounding closed surface. For both the skyrmion and BP, we have q=$\pm$1.

In contrast to a skyrmion, the spin configuration of a ChB varies along its spine, and eventually exhibits a magnetic singularity BP at the termination point. Let us compare the motion of skyrmion and ChB. The size of a typical skyrmion is determined by spin interactions and is generally incommensurate with the lattice constant. Therefore, a skyrmion may be regarded as a smooth object, which moves steadily through the lattice under electric current without impurities. In contrast, BP, being a point singularity, is strongly affected by the atomic potentials. We, therefore, expect a significantly distinct dynamics of ChBs and a skyrmion.

In this article, we investigate the current-induced magnetic dynamics of a ChB in a chiral magnet. Unlike the constant Hall angle for skyrmions shown in Fig. S1[31], ChB exhibits tunable Hall effect by the current density, which arises due to the pinning force experienced by the BP in a periodic lattice. Motion of the BP through the periodic lattice potential generates dynamical modes with frequencies that can be

two orders of magnitude higher than those of a skyrmion. We propose a simplified "spring-oscillator" model, in which we treat ChB as a composite object consisting of a BP and a skyrmion connected by an elastic spring. It allowed us to interpret the unconventional dynamics of ChBs.

Current-driven ChB dynamics

We performed numerical calculations using the micromagnetic simulation code Mumax3[32]. The total micromagnetic energy density is

$$\varepsilon = A(\nabla \boldsymbol{m})^2 + D\boldsymbol{m} \cdot (\nabla \times \boldsymbol{m}) - \mu_0 M_s \boldsymbol{H}_{ex} \cdot \boldsymbol{m} - \frac{1}{2}\mu_0 M_s \boldsymbol{H}_{dm} \cdot \boldsymbol{m} \qquad (2)$$

where A and D are Heisenberg exchange constant and the Dzyaloshinskii – Moriya interaction (DMI) constant, respectively. The parameters M_s, H_{ex} and H_{dm} are the saturation magnetization, external magnetic and demagnetizing fields, respectively. It should be noted that the BP itself cannot be treated within the framework of micromagnetism. Nevertheless, micromagnetic simulations can reliably describe the magnetization dynamics in the vicinity of the BP. That allows to infer the motion of BP thereafter[6] and feed the discrete potential imitating atomic lattice[6,10] to the dynamics of BP. One should be careful with the limits of micromagnetic approximation: (i) an exact correspondence with atomistic simulations and experiments should not be expected; (ii) it can be only used to study a cubic lattice.

The magnetization dynamics was calculated by solving the Landau-Lifshitz-Gilbert (LLG) equation with the spin transfer torque (STT) terms:

$$\frac{\partial \boldsymbol{m}}{\partial t} = -\gamma \boldsymbol{m} \times \boldsymbol{B}_{\text{eff}} + \frac{\alpha}{m}\boldsymbol{m} \times \frac{\partial \boldsymbol{m}}{\partial t} - u(\boldsymbol{j} \cdot \nabla)\boldsymbol{m} + \frac{\beta u}{m}\boldsymbol{m} \times (\boldsymbol{j} \cdot \nabla)\boldsymbol{m} \qquad (3)$$

where γ is the gyromagnetic ratio, α is the Gilbert damping constant, $\boldsymbol{j}$ is the STT current density, β is the nonadiabatic parameter, B_{eff} is the effective magnetic field. The coefficient $u = \frac{Pa^3}{2em}$ is the spin current velocity, where P is the spin polarization, a is the lattice constant, e and m are the elementary charge and mass, respectively.

A 900×900×90 nm^3 system with two-dimensional periodic boundary conditions was used to avoid the boundary effects. To stabilize a ChB, the thickness of the magnetic film was set to be larger than the period of the incommensurate spin spiral. The following material parameters of chiral magnet FeGe were used in our simulations: A=8.78 pJ/m, D=1.58 mJ/m^2, and M_s=385 kA/m[33]. The damping coefficient α was set to 0.05. A stable ChB with $L_d = 70$ nm and $L_p = 48$ nm was obtained by relaxing a conical system with a Bobber-like initial state.

The in-plane displacement of the ChB is determined by the position of the surface skyrmion (SS), which is fitted by the two-dimensional topological charge density on the top layer. The current is applied along the x-axis and the cell size is set to 3×3×3 nm^3. Fig. 2a and 2b show the calculated velocities $v_{\parallel}$ (parallel to j) and $v_{\perp}$ (perpendicular to j) versus the current density j for the skyrmion tube (blue lines) and ChB (red lines), respectively. In contrast to the universal linear j-v characteristics of skyrmion tube, ChB exhibits a rather complex nonlinear behavior. At low current density j, where the skyrmion tube has a steady motion, the ChB does not move. The result indicates that the ChB is pinned while the skyrmion tube suffers almost no pinning effect. Since the only difference between the ChB and the skyrmion tube is the presence of the BP, we infer that the conspicuous pinning behavior of the ChB is

induced by the BP. In the range of current densities j_{c1}~0.9×10^7 A/cm^2 to j_{c2}~1×10^7 A/cm^2, ChB starts to move with non-zero $v_\perp$, whereas the longitudinal velocity remains zero $v_\parallel$=0. At higher j, the longitudinal velocity $v_\parallel$ is activated and the j-v characteristics of ChB show similar tendency to that of skyrmion with an offset. At the connection point, we observe a sudden drop of $v_\perp$.

The Hall effect of ChB is different from that of skyrmion, who's the Hall angle is insensitive to the current density for an impurity-free magnetic system[17,34]. Fig. 2c shows the dependence of Hall angle θ on the current density for several values of β/α=0.5, 1.0, 2.0. For $j_{c1}< j<j_{c2}$, the ChB Hall angle is θ=-90° (the minus sign means clockwise). For $j>j_{c2}$, the Hall angle θ decreases quickly with increasing current density j. At higher current, the Hall angle θ approaches an asymptotic value, and we notice a small difference between the value and the skyrmion Hall angle. The difference will be addressed in the following analysis.

To understand this unique relation between θ and j, we further adopted Thiele's approach[34-36]. By assuming the rigidity of spin texture during the motion, the LLG equation can be projected onto a translational mode. For the skyrmion, the Thiele's equation is written as

$$\boldsymbol{G} \times \left(\boldsymbol{v}_j - \boldsymbol{v}_d\right) + \boldsymbol{\mathcal{D}}\left(\beta \boldsymbol{v}_j - \alpha \boldsymbol{v}_d\right) + \boldsymbol{F}_{ip} = 0, \qquad (4)$$

Where $\boldsymbol{v}_j$ is the velocity of conduction electrons and $\boldsymbol{v}_d$ is the drift velocity of the skyrmion. The first term indicates the Magnus force with the gyromagnetic coupling vector $\boldsymbol{G} = (0, 0, \mathcal{G})$ where $\mathcal{G} = 4\pi \mathrm{q}$. The second term is the dissipative force, and the components of the dissipation tensor $\boldsymbol{\mathcal{D}}$ are given by $\boldsymbol{\mathcal{D}} = \begin{pmatrix} \mathcal{D} & 0 \\ 0 & \mathcal{D} \end{pmatrix}$. The third term

$\boldsymbol{F}_{ip}$ is the phenomenological pinning force due to the impurities and is zero for a clean magnetic system.

To extend the Thiele's approach to ChB, we model a ChB as a composite particle consisting of SS and BP coupled via some phenomenological elastic force. BP is pinned by the lattice potential[6]. We assume that BP is dragged by the elastic force from the SS rather than the STT. When the SS is coupled with BP, the Thiele's equation can be rewritten as:

$$\boldsymbol{G} \times \left(\boldsymbol{v}_j - \boldsymbol{v}_d\right) + \boldsymbol{\mathcal{D}}\left(\beta\, \boldsymbol{v_j} - \alpha\, \boldsymbol{v}_d\right) + \boldsymbol{F}_{bp}(\boldsymbol{v}_d) = 0. \qquad (5)$$

The term $\boldsymbol{F}_{bp}(\boldsymbol{v}_d)$ represents friction and originates from the pinning of the BP by the periodic lattice potential. Using phenomenological arguments[17], the friction force $\boldsymbol{F}_{bp}(\boldsymbol{v}_d)$ is expected to satisfy the following conditions: (i) it is antiparallel to the drift velocity $\boldsymbol{v}_d$, (ii) it approaches finite (non-vanishing) value as $v_d \to 0$ due to pinning, (iii) it scales as $\propto v_d$ as $v_d \to \infty$. To this end, we adopt the following expression:

$$\boldsymbol{F}_{bp}(\boldsymbol{v}_d) = -\lambda\, \boldsymbol{v}_d \sqrt{1 + \left(\frac{v_{pin}}{v_d}\right)^2}. \qquad (6)$$

Here v_{pin} is the phenomenological parameter (with units of velocity) describing pinning of the Bloch point by the lattice potential. In the first approximation, v_{pin} is a scalar, which does capture the anisotropy of the lattice. The dimensionless parameter λ accounts for the effective scale of BP with respect to the skyrmion. The strength of $\boldsymbol{F}_{bp}(\boldsymbol{v}_d)$ can be represented by the displacement between the SS and BP, shown in Fig. S2[31], according to the Hooke's law $\boldsymbol{F}(\boldsymbol{v}_d) = k\Delta\boldsymbol{r}(\boldsymbol{v}_d)$.

Let us first examine the limiting case for large velocity $v_d \gg v_{pin}$, where the friction force (6) is approximately $\boldsymbol{F}_{bp}(\boldsymbol{v}_d) \approx -\lambda\, \boldsymbol{v}_d$. Plugging that expression in Eq. (5) and solving the latter for the tangent of the Hall angle $\tan\theta = \frac{v_\perp}{v_\parallel}$, we find

$$\tan\theta = \frac{(\alpha^*-\beta)\mathcal{D}\mathcal{G}}{\mathcal{G}^2+\alpha^*\beta\mathcal{D}^2}, \qquad (7)$$

where $\alpha^* = \alpha + \frac{\lambda}{\mathcal{D}}$. It implies that the Hall angles of ChB and skyrmion ($\tan\theta = \frac{(\alpha-\beta)\mathcal{D}\mathcal{G}}{\mathcal{G}^2+\alpha\beta\mathcal{D}^2}$) are distinct at high current. Note that $\tan\theta$ changes sign at $\alpha^* = \beta$, and, so, α^* may be extracted from the numerical modeling.

In the opposite limit of small velocity $v_d \ll v_{pin}$, the friction force is approximately $\boldsymbol{F}_{bp}(v_d) \approx -\frac{\lambda v_{pin}\, \boldsymbol{v}_d}{v_d}$. The solution of Eq. (5) gives rise to the following v_d and θ.

$$v_d = \frac{-\alpha\mathcal{D}\lambda v_{pin}+\sqrt{H_\alpha H_\beta v_j^2-\mathcal{G}^2\lambda^2 {v_{pin}}^2}}{H_\alpha}, where\ v_j \geq \frac{\lambda v_{pin}}{H_\beta}$$

$$v_\parallel = \frac{H_{\alpha\beta}v_d^2+\beta\mathcal{D}\lambda v_d v_{pin}}{(\alpha\mathcal{D}v_d+\lambda v_{pin})^2+\mathcal{G}^2 v_d^2} v_j$$

$$v_\perp = \frac{(\beta-\alpha)\mathcal{G}D\mathcal{D}+\mathcal{G}\lambda v_d v_{pin}}{(\alpha\mathcal{D}v_d+\lambda v_{pin})^2+\mathcal{G}^2 v_d^2} v_j$$

$$tan\,\theta = \frac{\mathcal{D}\mathcal{G}(\alpha-\beta)H_{\alpha\beta}v_j^2+\mathcal{G}\lambda v_{pin}\sqrt{H_\alpha H_\beta v_j^2-\mathcal{G}^2\lambda^2 {v_{pin}}^2}}{{H_{\alpha\beta}}^2 v_j^2-\mathcal{G}^2\lambda^2 {v_{pin}}^2} \qquad (8)$$

Here $H_\alpha = \alpha^2\mathcal{D}^2 + \mathcal{G}^2$, $H_\beta = \beta^2\mathcal{D}^2 + \mathcal{G}^2$, $H_{\alpha\beta} = \alpha\beta\mathcal{D}^2 + \mathcal{G}^2$. The fitting data are plotted in Fig.2c with blue solid lines.

Note that relation (8) is universal except for $j<j_{c2}$, which is analogous to static friction zone. In the small current limit, the analytical formulas (8) do not provide a reliable description of numerical results because the lattice symmetry confines the BP relatively stronger. Our qualitative understanding of ChB dynamics in that limit is as follows. Our micromagnetic grid is equivalent to a simple cubic lattice. At small

current density applied in *x*-direction, the ChB has a stronger tendency of large Hall angle following relation (8). And, so, it is easier to overcome the barrier along the *y*-axis in the discrete lattice potential and the Hall angle is always -90° until the barrier along the *x*-axis is overcome. In this region $j_{c1}<j<j_{c2}$, the stretch of ChB cannot be released by BP moving along the *x*-axis. Therefore, $v_{\perp}$ is enhanced by a compensation from losing $v_{\parallel}$. When $j>j_{c2}$, $v_{\parallel}$ is activated. The compensation vanishes, and the motion behavior reduces to relation (8).

Considering the discreteness of lattice and relative spatial positions of SS and BP, we conjecture that although confined by the surface of plate, the ChB has more complex dynamics in the three-dimensional space, which can be visualized by the motion of BP. Fig. 3a shows the position of BP in *x, y* and *z* direction over time for the current density of $j=5\times10^7$ A/cm^2 with the inset showing the time range from 10 to 12 ns. The position of BP is defined as the center of the local three-dimensional topological charge density and this can be estimated by the local charge density distribution around the BP. This method provides a more reliable estimate of BP's position in three spatial dimensions. In the *x* and *y* directions, the motion of BP shows a step-wise behavior, and the distance of each step is the cell size 3 nm. Interestingly, BP shows high frequency oscillations in *z*-direction, although ChB is only excited by an in-plane current. The amplitude is less than the cell size indicating the absence of significant deformation on ChB. The periods of the oscillations are related to the in-plane lattice potential. We also find the magnetic dynamic modes of ChB are related to the motion of BP, which can be seen in the frequency domain shown in Fig. 3b.

The fast Fourier transformations (FFT) of *z* coordinate of BP and the *z* component of the total magnetization are used to analyze the frequency spectra. The frequencies of main peaks are aligned, suggesting that the magnetic dynamic modes of ChB are excited by the lattice pinning effect of BP. The frequencies of these modes range from 0.75 GHz to about 10 GHz which is higher than skyrmion tube (about 0.36 GHz[31]).

Taking into account the periodicity of the lattice potential $\boldsymbol{V}(x,y) = \boldsymbol{V}(x + n_{\parallel}a, y + n_{\perp}b)$ and the ChB moves from $\boldsymbol{r}_0(0,0,0)$ to $\boldsymbol{r}_1(x,y,0)$ in Δt time, the frequencies can be estimated:

$$f_{\parallel} = \frac{n_{\parallel}}{\Delta t} = \frac{x}{a\Delta t} = \frac{v_{\parallel}}{a}$$

$$f_{\perp} = \frac{n_{\perp}}{\Delta t} = \frac{x}{b\Delta t} = \frac{v_{\perp}}{b} \qquad (9)$$

where $n_{\parallel}$ and $n_{\perp}$ are the numbers of cells in directions parallel and perpendicular to $\boldsymbol{j}$ between $\boldsymbol{r}_0$ and $\boldsymbol{r}_1$, respectively; a and b are lattice constants. Here the average velocity of BP is $v_{\parallel}$ ≈23.8 m/s and $v_{\perp}$ ≈2.25 m/s. The calculated frequencies are $f_{\parallel} =$ 7.9 GHz and $f_{\perp} = 0.75$ GHz, which are in good agreement with the numerical results indicated by arrows in the Fig. 3b. The peaks besides the two calculated frequencies are high order harmonics. According to this formula, we predict that ChB could have a dynamical mode with an extremely high frequency about 0.14 THz for a higher velocity (∼100 m/s) and smaller cell size (∼0.7 nm for real FeGe lattice). We note that a too small cell size is beyond the applicability of micromagnetic approximation, so the extrapolated value is a reference. More accurate results for the actual crystal lattice may be obtained from atomistic simulations or direct experiments.

So, the phenomenological "spring oscillator" model of ChB allowed to explain the simulated results quite well. The motion process of a ChB is shown schematically in the Figs. 3c. When the ChB is driven, a pinning force of BP by the lattice is induced, giving rise to the different trajectory of ChB from that of skyrmion and high frequency BP mode. Because the BP is pinned by the lattice, the ChB is stretched, and an internal tension pulls the BP forward and up in space. When the BP jumps into the next cell, the internal tension is released, and the BP relaxes back. Therefore, the *z* coordinate of BP changes periodically, and the BP dynamical modes are excited.

Fig. 4a shows the results in the frequency domain for different currents and fixed cell size 3×3×3 nm^3. The major frequencies change with the current density significantly and the frequency at j=9×10^7 is nearly 20 GHz, which is two orders of magnitude higher than that of a skyrmion tube. Fig. 4b shows the linear fitting of the current-dependent frequency. The tendency of frequency change is consistent with Eq. (9). The intercepts are non-zero because the ChB can move only if the current density is greater than the critical current j_{c1} for $v_\perp$ and j_{c2} for $v_\parallel$. Fig. 4c and 4d show the dependency of cell sizes on the frequency with fixed current density 5×10^7 A/cm^2. The frequencies increase with decreasing cell size, which is also consistent with Eq. (9). A mode with a frequency of 0.4 GHz does not vary with the cell size. This mode is similar to the breathing mode of a skyrmion.

Conclusion

We investigate the current-induced dynamics of ChB numerically. We find that ChB can be regarded as a composite particle consisting of SS and BP. Therefore, ChB

has a different dynamical behavior from that of skyrmion. Current-density-dependent ChB Hall effect and new dynamical modes induced by the pinning effect of BP were discovered. The ChB Hall angle can be adjusted in a wide range by the applied current density. The range of BP mode frequencies varies by at least two orders of magnitudes. A simple spring-oscillator-like model was employed to address these observations. Further experimental methods such as the topological Hall effect measurements, spin wave detections, or 3D x-ray tomography could be performed to verify our numercial results. The rich dynamics of ChB provides an opportunity to explore spin wave and other spintronic applications.

Acknowledgements

This work is supported by the National Key Research Program of China (Grant Nos. 2016YFA0300701, 2017YFB0702702, and 2018YFF01010303), the National Natural Sciences Foundation of China (Grant Nos. 1187411, 52031015, 51427801 and 11804343) and the Key Research Program of Frontier Sciences, CAS (Grant Nos. QYZDJ-SSW-JSC023, KJZD-SW-M01 and ZDYZ2012-2). Work at UNH was supported by the Office of Basic Energy Sciences, Division of Materials Sciences and Engineering, U.S. Department of Energy, under award no. DE-SC0020221.

References

[1] F. N. Rybakov, A. B. Borisov, S. Blügel, and N. S. Kiselev, Phys. Rev. Lett. **115**, 117201 (2015).

[2] F. Zheng, F. N. Rybakov, A. B. Borisov, D. Song, S. Wang, Z.-A. Li, H. Du, N. S. Kiselev, J. Caron, A. Kovács, M. Tian, Y. Zhang, S. Blügel, and R. E. Dunin-Borkowski, Nat. Nanotechnol. **13**, 451 (2018).

[3] A. S. Ahmed, J. Rowland, B. D. Esser, S. R. Dunsiger, D. W. McComb, M. Randeria, and R. K. Kawakami, Phys. Rev. Mater. **2**, 041401(R) (2018).
[4] S. Mühlbauer, B. Binz, F. Jonietz, C. Pfleiderer, A. Rosch, A. Neubauer, R. Georgii, and P. Böni, Science **323**, 915 (2009).
[5] X. Z. Yu, Y. Onose, N. Kanazawa, J. H. Park, J. H. Han, Y. Matsui, N. Nagaosa, and Y. Tokura, Nature (London) **465**, 901 (2010).
[6] S. K. Kim and O. Tchernyshyov, Phys. Rev. B **88**, 174402 (2013).
[7] M. Y. Im, H. S. Han, M. S. Jung, Y. S. Yu, S. Lee, S. Yoon, W. Chao, P. Fischer, J. I. Hong, and K. S. Lee, Nat. Commun. **10**, 593 (2019).
[8] M. Charilaou, Phys. Rev. B **102**, 014430 (2020).
[9] M. Beg, R. A. Pepper, D. Cortés-Ortuño, B. Atie, M.-A. Bisotti, G. Downing, T. Kluyver, O. Hovorka, and H. Fangohr, Sci. Rep. **9**, 7959 (2019).
[10] Y. Li, L. Pierobon, M. Charilaou, H.-B. Braun, N. R. Walet, J. F. Löffler, J. J. Miles, and C. Moutafis, Phys. Rev. Research **2**, 033006 (2020).
[11] J. Zhu, Y. Wu, Q. Hu, L. Kong, J. Tang, M. Tian, and H. Du, Sci. China Phys. Mech. **64**, 227511 (2020).
[12] K. Ran, Y. Liu, Y. Guang, D. M. Burn, G. v. d. Laan, T. Hesjedal, H. Du, G. Yu, and S. Zhang, Phys. Rev. Lett. **126**, 017204 (2021).
[13] X. Z. Yu, N. Kanazawa, W. Z. Zhang, T. Nagai, T. Hara, K. Kimoto, Y. Matsui, Y. Onose, and Y. Tokura, Nat. Commun. **3**, 988 (2012).
[14] S. X. Huang and C. L. Chien, Phys. Rev. Lett. **108**, 267201 (2012).
[15] Y. Onose, Y. Okamura, S. Seki, S. Ishiwata, and Y. Tokura, Phys. Rev. Lett. **109**, 037603 (2012).
[16] J. Sampaio, V. Cros, S. Rohart, A. Thiaville, and A. Fert, Nat. Nanotechnol. **8**, 839 (2013).
[17] J. Iwasaki, M. Mochizuki, and N. Nagaosa, Nat. Commun. **4**, 1463 (2013).
[18] R. Tomasello, E. Martinez, R. Zivieri, L. Torres, M. Carpentieri, and G. Finocchio, Sci. Rep. **4**, 6784 (2014).
[19] H. Du, R. Che, L. Kong, X. Zhao, C. Jin, C. Wang, J. Yang, W. Ning, R. Li, C. Jin, X. Chen, J. Zang, Y. Zhang, and M. Tian, Nat. Commun. **6**, 8504 (2015).
[20] X. Zhang, G. P. Zhao, H. Fangohr, J. P. Liu, W. X. Xia, J. Xia, and F. J. Morvan, Sci. Rep. **5**, 7643 (2015).
[21] N. Ogawa, S. Seki, and Y. Tokura, Sci. Rep. **5**, 9552 (2015).
[22] W. Jiang, X. Zhang, G. Yu, W. Zhang, X. Wang, M. Benjamin Jungfleisch, John E. Pearson, X. Cheng, O. Heinonen, K. L. Wang, Y. Zhou, A. Hoffmann, and Suzanne G. E. te Velthuis, Nature Phys. **13**, 162 (2016).
[23] K. Litzius, I. Lemesh, B. Krüger, P. Bassirian, L. Caretta, K. Richter, F. Büttner, K. Sato, O. A. Tretiakov, J. Förster, R. M. Reeve, M. Weigand, I. Bykova, H. Stoll, G. Schütz, G. S. D. Beach, and M. Kläui, Nature Phys. **13**, 170 (2016).
[24] H. Fujita and M. Sato, Phys. Rev. B **95**, 054421 (2017).
[25] F. Zheng, H. Li, S. Wang, D. Song, C. Jin, W. Wei, A. Kovács, J. Zang, M. Tian, Y. Zhang, H. Du, and R. E. Dunin-Borkowski, Phys. Rev. Lett. **119**, 197205 (2017).

[26] H. Du, X. Zhao, F. N. Rybakov, A. B. Borisov, S. Wang, J. Tang, C. Jin, C. Wang, W. Wei, N. S. Kiselev, Y. Zhang, R. Che, S. Blügel, and M. Tian, Phys. Rev. Lett. **120**, 197203 (2018).
[27] P. Padmanabhan, F. Sekiguchi, R. B. Versteeg, E. Slivina, V. Tsurkan, S. Bordács, I. Kézsmárki, and P. H. M. van Loosdrecht, Phys. Rev. Lett. **122**, 107203 (2019).
[28] Y. Liu, R. K. Lake, and J. Zang, Phys. Rev. B **98**, 174437 (2018).
[29] Y. Liu, W. Hou, X. Han, and J. Zang, Phys. Rev. Lett. **124**, 127204 (2020).
[30] N. Kent, N. Reynolds, D. Raftrey, I. T. G. Campbell, S. Virasawmy, S. Dhuey, R. V. Chopdekar, A. Hierro-Rodriguez, A. Sorrentino, E. Pereiro, S. Ferrer, F. Hellman, P. Sutcliffe, and P. Fischer, Nat. Commun. **12**, 1562 (2021).
[31] See Supplemental Material for details of the comparison to skyrmion and the numerical evidence for the elastic force in a ChB.
[32] A. Vansteenkiste, J. Leliaert, M. Dvornik, M. Helsen, F. Garcia-Sanchez, and B. V. Waeyenberge, AIP Adv. **4**, 107133 (2014).
[33] M. Beg, R. Carey, W. Wang, D. Cortés-Ortuño, M. Vousden, M.-A. Bisotti, M. Albert, D. Chernyshenko, O. Hovorka, R. L. Stamps, and H. Fangohr, Sci. Rep. **5**, 17137 (2015).
[34] K. Everschor, M. Garst, B. Binz, F. Jonietz, S. Mühlbauer, C. Pfleiderer, and A. Rosch, Phys. Rev. B **86**, 054432 (2012).
[35] A. A. Thiele, Phys. Rev. Lett. **30**, 230 (1973).
[36] K. Everschor, M. Garst, R. A. Duine, and A. Rosch, Phys. Rev. B **84**, 064401 (2011).

Figures and captions

Figure 1

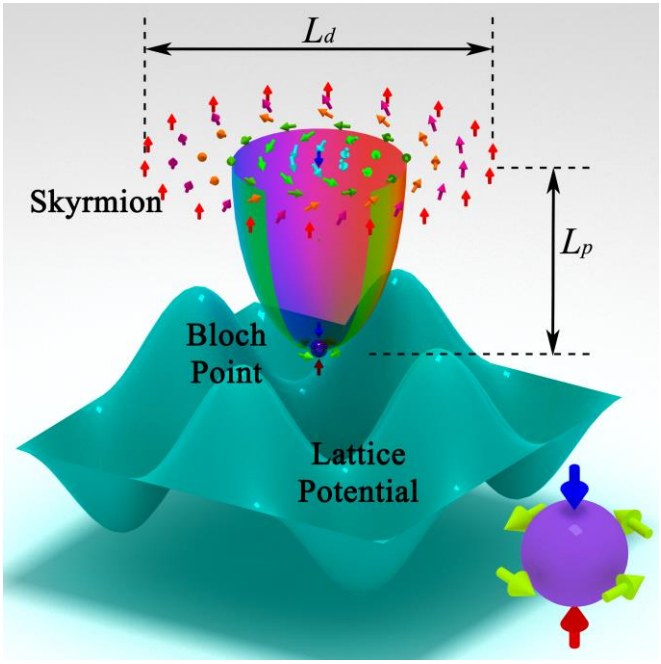

FIG. 1 (color online). Cartoon representation of a Chiral Bobber (ChB) and the Bloch Point (BP) pinned by the lattice potential. The inset illustrates spin configuration around the BP.

Figure 2

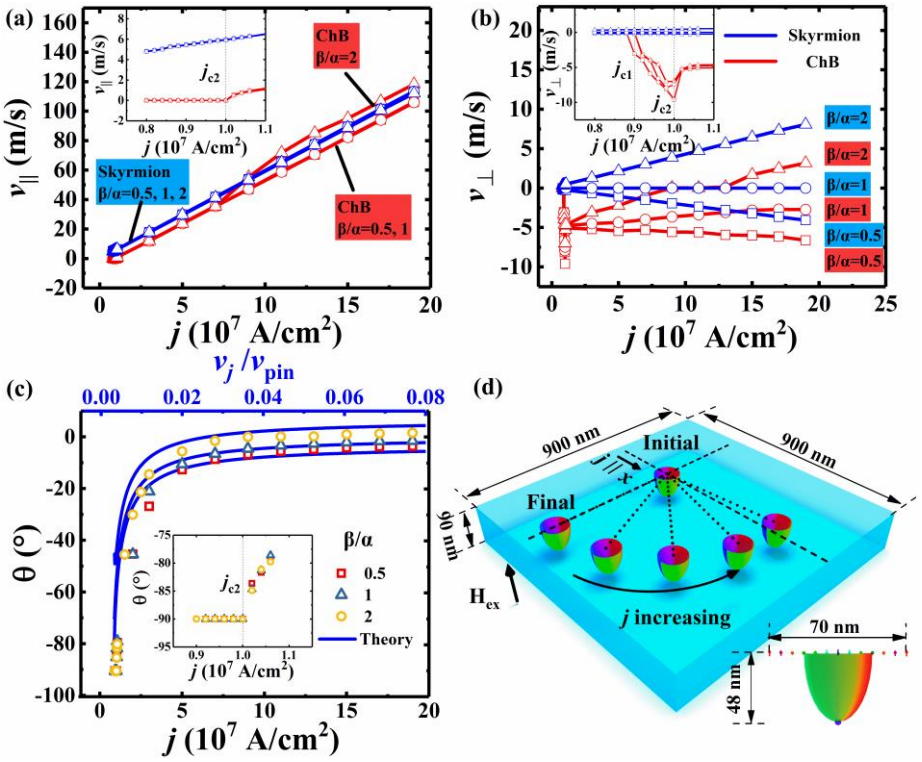

FIG. 2 (color online). Dynamics of ChB in the presence of the electrical current applied in the x direction. (a) (b) The longitudinal and transverse velocities of ChB and skyrmion tube with different current density for fixed β/α=0.5, 1.0, 2.0. The insets are the magnifications of the region at low current density. (c) The dependence of ChB Hall angle on the current density for fixed β/α=0.5, 1.0, 2.0. The dots represent the results of simulation, and the solid lines represent the calculated results by Thiele's equation. Values of other parameters $\mathcal{G} = -4\pi, \mathcal{D} = 9.4\pi, \lambda = 0.04$. The inset is the magnification of the region at low current density. (d) The schematics of the current driven ChB trajectories at β/α=2. The curved arrow indicates the evolution of ChB trajectory with current density increasing. The inset shows the ChB size before current applied.

Figure 3

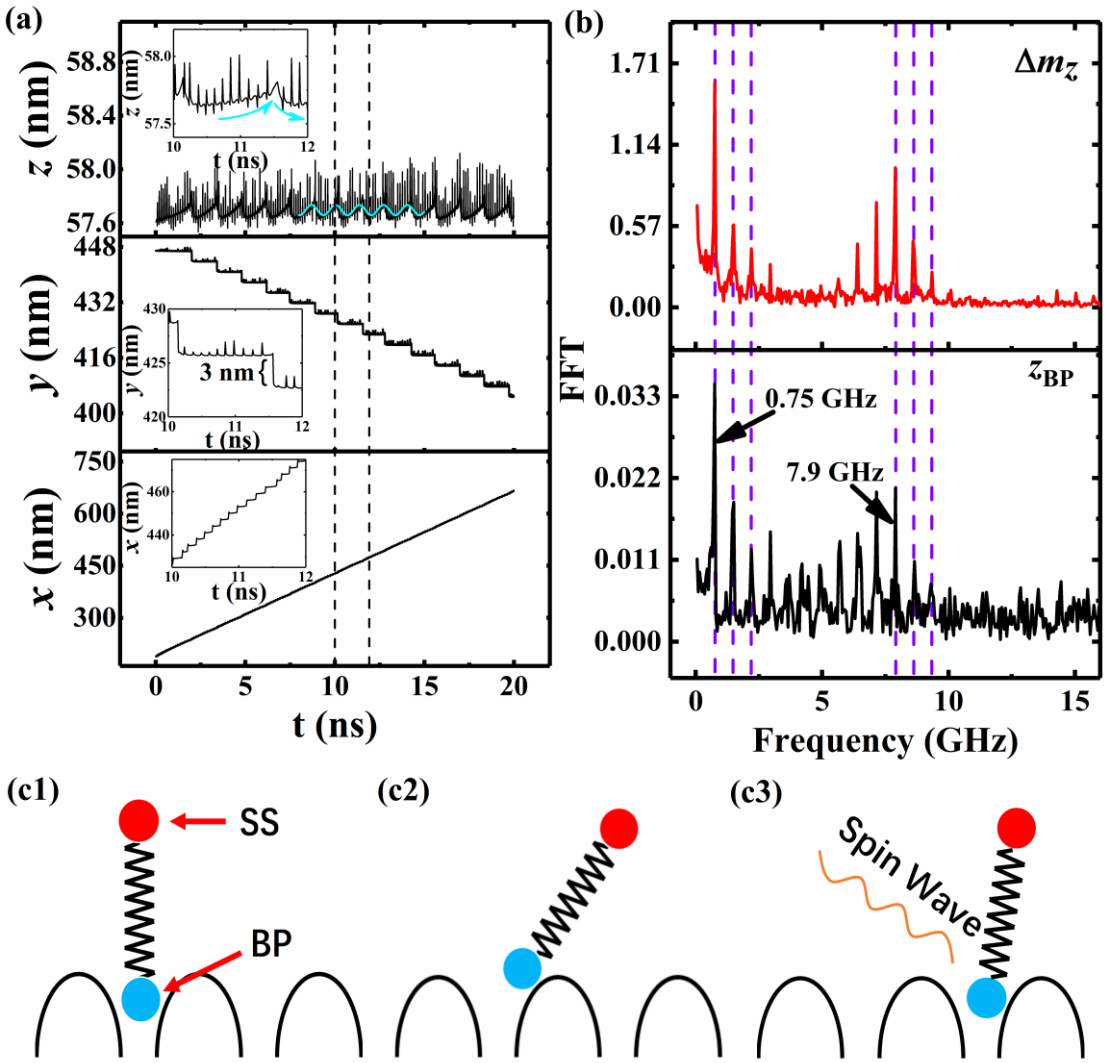

FIG. 3 (color online). (a) Time dependence of x, y, and z positions of BP in the 3D Cartesian coordinate system with the current density 5×10^7 A/cm^2. Insets: the magnification in the range of 10 to 12 ns; the cyan curve is a guide for the eyes of the period related to the y component of the lattice potential. (b) The fast Fourier transformation (FFT) for the z position of BP and the z component of the total magnetization over time. (c) Schematic diagram of ChB motion process: (c1) The initial state before the current is applied; (c2) The intermediate state in which the ChB is stretched; (c3) The final state in which the BP relaxes back.

Figure 4

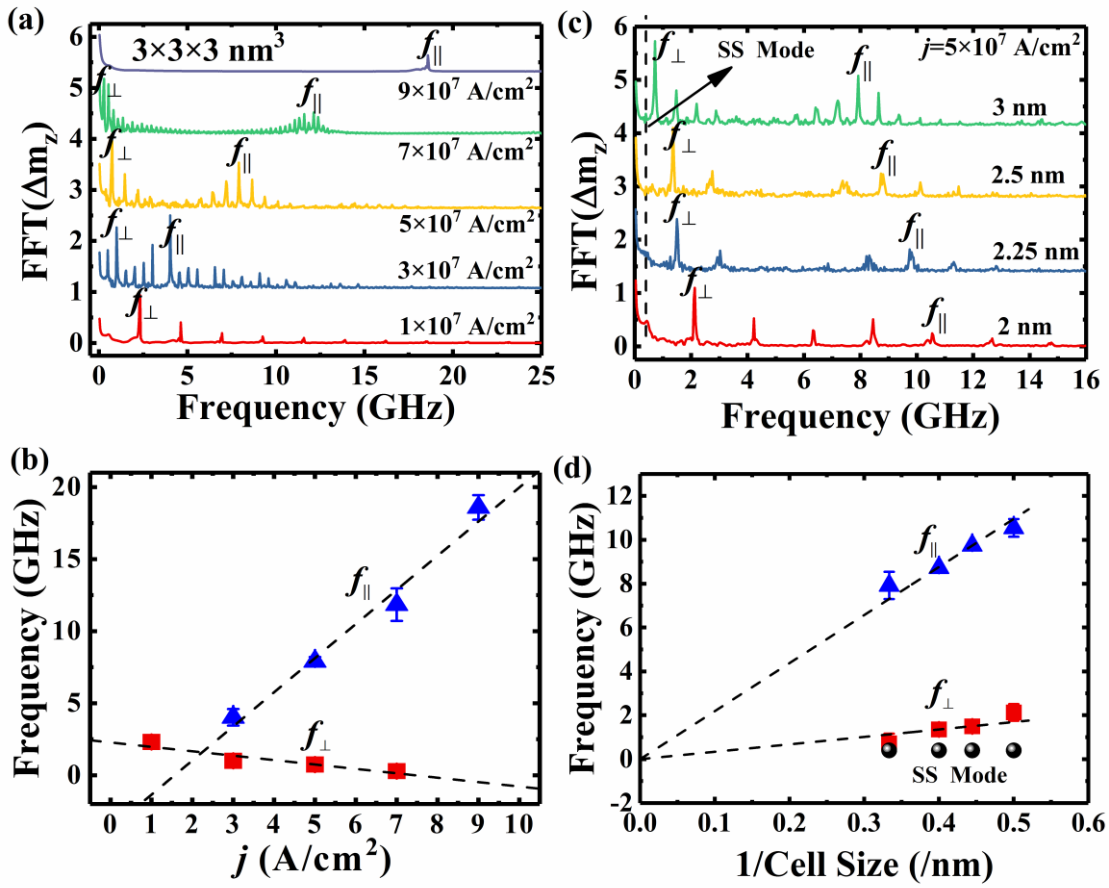

FIG. 4 (color online). (a) The frequency spectra of ChB at different current densities for the fixed cell size 3×3×3 nm^3. (b) The current density dependence of frequency: the dashed lines are the linear fittings. (c) The frequency spectra of ChB for different cell size with the fixed current density 5×10^7 A/cm^2. The dashed line indicates the peak position of the low frequency SS mode. (d) The dependence of frequency on the 1/cell size: the dashed lines are the linear fittings; the black balls are the SS mode with frequency f=0.4 GHz.